https://doi.org/10.1016/j.ijheatmasstransfer.2018.11.082

Numerical study on Indirect Evaporative Coolers considering condensation: A thorough comparison between cross flow and counter flow

Min Yunran[1], Chen Yi[2*] and Yang Hongxing[1*]

1 Renewable Energy Research Group (RERG), Department of Building Services Engineering, The Hong Kong Polytechnic University, Hong Kong

2 Faculty of Science and Technology, Technological and Higher Education Institute of Hong Kong, Hong Kong

Abstract

Indirect evaporative cooling is recognized as an alternative air-cooling solution with low carbon potential and considerable energy efficiency. An indirect evaporative cooler (IEC) can handle both of the sensible and latent cooling loads because of possible condensation when it is used as a precooling unit in an air-conditioning system in hot and humid regions. Cross flow and counter flow, as two basic flow configurations of an IEC, differ in condensation behavior that affects their cooling performance. In this paper, a novel 2-D model of cross flow IEC considering condensation is established and validated. The performance of the cross flow and counter flow IEC is thoroughly compared under the same configuration. The channel gap and height to length ratio (H/L) are optimized to provide references for the design and operation of the IEC under condensation conditions. Results show that under the same operating conditions, the condensation ratio of counter flow IEC is 2%~15% higher than that of the cross flow IEC, leading to 2~7% decrease of wet-bulb effectiveness. The difference in the total heat transfer rate between the two configurations is less than 5% when the number of transfer units (NTU_p) is lower than 3.1. For cross flow IEC, there is an optimal value in H/L among 0.4~0.8 considering the cooling capacity and energy consumption.

Key words: Indirect evaporative cooler, Cross flow, Counter flow, Condensation, Numerical simulation, Optimization

Nomenclatures		Greek letters	
r	condensation ratio	ω	humidity ratio of mist air, kg/kg
c_p	the specific heat capacity, kJ/(kg·℃)	ε	efficiency
c_{pa}	the specific heat capacity of moist air, kJ/(kg·℃)	η	wet-bulb effectiveness
c_{pw}	the specific heat capacity of water, kJ/(kg·℃)	ρ	density, kg/m^3
H	height of heat exchanger, m	σ	surface wettability
L	length of the heat exchanger, m	υ	kinematic viscosity, m^2/s
s	channel gap, m	μ	dynamic viscosity, Pa·s
n	number of channels	Subscripts	
m	air mass flow rate, kg/s	s	secondary air

* Corresponding author.
E-mail address: yichen@vtc.edu.hk (Y. Chen); hong-xing.yang@polyu.edu.hk (H. Yang)

h	heat transfer coefficient, W/m^2·℃	p	primary air
h_m	mass transfer coefficient, kg/m^2·s	w	water film
A	heat exchange area, m^2	d	dry air
A_{con}	wetted surface area by condensation water	t_w	water temperature
h_{fg}	latent heat of vaporization of water, kJ/kg	dew	dew point temperature
h_{fg}^0	latent heat of vaporization of water at reference temperature (0℃)	v	water vapor
T	thermodynamic temperature, K	q_b	saturation vapor pressure
t	temperature, ℃	c	condensation
i	enthalpy of moist air, kJ/kg	e	evaporation
Re	Reynolds number	wb	wet-bulb
NTU	number of heat transfer unit	sat	saturated humidity
d_e	hydraulic diameter of channel, m	in	inlet of air channel
COP	coefficient of performance	out	outlet of air channel
f_{Re}	friction coefficient	sen	sensible heat
u	air flow velocity, m/s	lat	latent heat
ΔP	total pressure drop		
K	motor capacity coefficient		
g	gravity acceleration, m/s^2		
q	heat transfer rate per unit mass, kW/kg		
E_{saving}	energy saving of IEC, W		
E_{net}	net energy saving of IEC, W		

1. Introduction

Building energy consumption has widely increased over the past few decades, of which the air conditioning systems take up to 50% of the total energy consumption in Hong Kong, and it is still a growing market [1-3]. The extensive electricity consumption of conventional mechanical cooling cycles posed a huge threat to the energy shortage and environmental issues, along with the consequent critical load on the power grid under summer conditions. Currently, many efforts have been made to develop sustainable technologies for air cooling solutions. As a kind of passive cooling technique, the indirect evaporative cooling costs lower energy consumption and reduces greenhouse gas emissions with no CFCs usage. This type of air treatment has gained fast development in recent decades, and are currently being used in different types of buildings [4].

The Indirect Evaporative Cooler (IEC) uses water evaporation to lower the dry-bulb temperature of the air, which means the wet-bulb temperature of intake air becomes a determinant that limits the supply air temperature. So far, IEC has been widely applied in hot and dry areas [5-7]. Due to the moderate humidity during summer conditions, it is achievable to produce low air temperature without a vapor compression refrigeration system. Under hot and humid climate conditions, coupled with additional cooling coils, IEC pre-cools the flesh air with exhausted air from air-conditioned spaces as a heat recovery system. In this way, the consumed energy and the size of the mechanical cooling units are reduced [8]. Recently, many novel indirect evaporative coolers and hybrid systems have been proposed [9-12], breaking the regional limitation for wider utilization.

The complexity of coupled heat and mass transfer on the evaporation film increases the difficulties of IEC modeling, which has been extensively studied. At first, analytical approaches were developed based on several hypotheses, such as linear approximate models of the specific enthalpy of the moist air [13], mean water surface temperature [14] and spray water enthalpy [15, 16]. To further explore the heat and mass mechanism within an IEC heat exchanger, numerical models were developed rapidly due to its improved accuracy. Finite difference method has been widely used to discretize the governing equations. Stefano et al. [17] developed a cross flow IEC model which take into account the actual wettability of heat exchanger surface and validated it through experiments conducted in typical data centers operating conditions. Wen et al. [18] built a mathematical model on the falling film shrinkage and investigated the effects of surfactants on the enhancements of wetting areas and the reduction of film thickness. Heidarinejad et al. [19-21] proposed a new model of IEC by taking the wall longitudinal heat conduction and spray water temperature variation into consideration. The governing equations are discretized by Finite difference method with which the forward difference scheme and central difference scheme were employed to solve the coupled equations iteratively. Finite differential approach with Newton iterative method based on EES (Engineering Equation Solver) software was also used in some studies [22-24]. Riangvilaikul et al. [24] investigated the theoretical performance of a novel dew point evaporative cooling system operating under various inlet air conditions. For other numerical methods, Lin et al. [3] put forward a mathematical model of counter flow IEC discretized by Finite Element method and simulated using COMSOL Multiphysics software. The performance in transient and steady-state were predicted and dominant factors in the cooling process were derived. Anisimov et al. [2, 25-27] presented a set of heat and mass transfer models with different air flow patterns and validated them by published experimental data. The numerical simulations were performed with the Runge-Kutta method with justified accuracy and stability. Wan et al. [28, 29] used a two-dimensional computational fluid dynamics (2-D CFD) model to simulate a counter flow indirect evaporative cooler by Finite Volume method. Second-order scheme was selected and SIMPLE algorithm

was used to solve the conservation equations. The obtained local Nusselt and Sherwood numbers are inputted to improve its accuracy.

With the development of numerical methods in solving the fluid flow and heat/mass transfer equations, the modeling of IECs has received great interests in these years by considering different factors such as surface wettability, spray water temperature variation, variable Lewis factor, and novel flow configurations. It can be observed from the previous works that the studies on IEC models were mostly with only sensible heat transfer being considered in primary air channels. The optimal operating conditions and preferable climatic zones of IEC were also investigated based on those models. However, when IEC is used in humid regions as a component of combined air cooling system to pre-cool the fresh air with the exhaust air from air-conditioned space, there is a high possibility of that condensation take place in primary air channels due to the high humidity of the fresh air. The condensation could lower the wet-bulb efficiency of IEC but improves the total heat transfer rate due to dehumidification. The performance of counter flow IEC with condensation from the primary air has been investigated by Chen et al. [30-32]. It is showed that the state of partial and total condensation account for 47.7% annual operation hours when a counter flow IEC hybrid cooling system applied in hot and humid regions. However, the discussion about IEC with cross flow pattern under condensation conditions has not been well addressed in the literature yet. The cross flow IEC is more commonly used in the current market because of easier air ducts arrangement and unit fabrication. However, the cross flow IEC model, based on two-dimensional heat and mass transfer, is more complicated than one dimensional counter flow IEC model. Besides, the energy performance, optimal structure and optimal operating parameters of cross flow IEC under condensation state will definitely be distinguished from that of counter flow IEC.

In this regard, this study will first develop a numerical model of cross flow IEC which takes the possible condensation from primary air into consideration. A thorough comparison between the cross flow and counter flow IEC under condensation state is made in terms of condensation ratio, wet-bulb efficiency and total heat transfer rate under different operational and geometrical parameters. Moreover, the optimal channel gap, height to length ratio (H/L) and number of transfer unit (NTU) will be proposed for both cross flow and counter flow IEC for their better application in hot and humid regions.

2. Description of cross-flow and counter flow IEC heat exchangers

2.1 Flow configurations

Two heat exchanging air streams in the IEC are namely primary and secondary air. According to the corresponding flow pattern, basic configurations of IEC can be classified into parallel, counter and cross

flow. The most common schematics of cross flow and counter flow plate type IEC are as shown in Fig. 1. In the cross-flow IEC, the inner surfaces of the secondary air channels are wetted by spraying water from the top of the heat exchanger, and the secondary air contact with water droplets directly in an upward direction, taking away the latent heat of the water film through water evaporation. The primary air in the dry channels flows along the horizontal direction of the heat exchanger and is cooled by the plate surfaces which covered by water film on the other side. While in a counter-flow IEC, the primary air passes vertically through the dry channels in a counter-flow pattern with the secondary air stream.

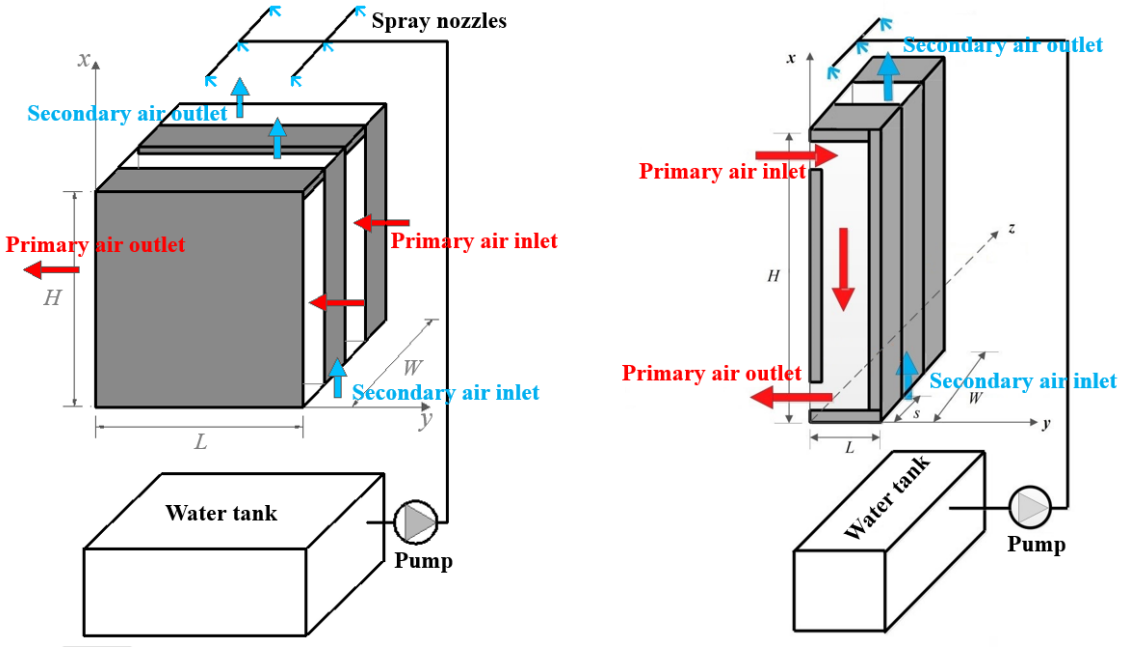

(a) Cross flow (b) Counter flow IEC

Fig. 1 Schematics diagram of plate type IEC

In terms of structure, the geometry of the separated air channels in counter flow IEC increase the difficulties to realize pure counter flow [10], while cross flow IEC is friendly to air ducts arrangement due to the compact structure. As for cooling performance, the optimal heat transfer performance of IEC is derived from counter flow pattern by approaching maximum temperature difference. In the same physical size and operation conditions, the counter-flow M-cycle heat exchangers can offer 20% greater cooling capacity and 23% higher wet-bulb effectiveness than the cross-flow pattern without considering condensation [22]. However, the differences between cross flow and counter flow IEC under condensation state have not been investigated. The cross flow and counter flow IEC could produce different temperature distributions on heat exchange plates, which influence the condensation rate in the primary air channels when the plate

temperature is below the dew point temperature of the inlet air stream. As a result, the cooling performance of cross flow and counter flow IEC may present a different result due to the condensation being involved.

2.2. Physical model

The modeling of counter flow IEC has been described elaborately in the previous work [30-32], so this paper would only present the modeling of cross flow IEC. As shown in Fig. 2, the primary air flows perpendicularly to the secondary air, and water is sprayed from top of the heat exchanger. The energy and mass balance of these three streams are basic principles that dominate the modeling process. When IEC is used as a heat recovery unit in an A/C system, the primary air is the fresh air to be cooled and the secondary air is the exhaust air from conditioned space. Therefore, the temperature and humidity of primary air from outdoor environment vary in certain ranges, and the secondary air from controlled indoor space can be regarded as relatively stable in temperature and humidity. The primary air conditions are based on the weather data in typical hot and humid regions. The secondary air conditions are based on the typical air conditions in A/C rooms. In this model, the considered ranges of governing parameters are: primary air temperature (26-42℃), humidity (30-90%), velocity (0.5-5.0 m/s); secondary air temperature (24-26℃), humidity (50-60%). Some assumptions are made in order to drive the mathematical models:

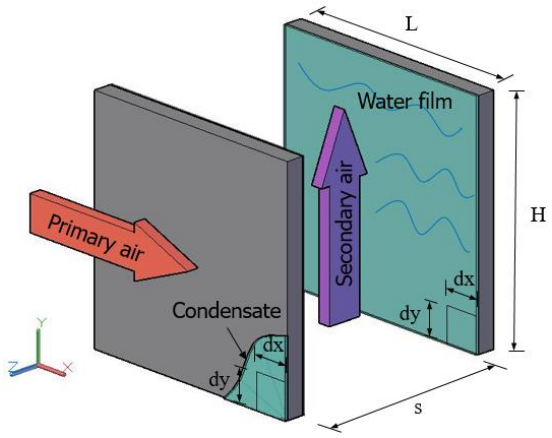

Fig. 2 Physical model of cross flow plate type IEC

1. The indirect evaporative cooler has no heat transfer with its surroundings.
2. Air flows are fully developed and the thermal properties of air and water are constant.
3. The water is distributed uniformly over the whole passages.
4. Both the water film and plate wall are very thin so the thermal resistances are negligible.
5. Lewis number is considered unity [33].
6. The water film is continuously replenished at the same temperature and the condensate water temperature is equal to the dew point temperature of the primary air;

7. Heat and mass are only transferred along the flow direction of the fluid;

2. Mathematical model of cross flow IEC considering condensation

2.1 2-D model equations

The present mathematical model developed to analyze the heat and mass transfer in cross flow IEC is based on the modified ε-NTU method [6, 10, 19]. In the present model, the possible condensation from primary air is taken into account. Conservation of the energy and mass for the elements presented in Fig.3 are as following:

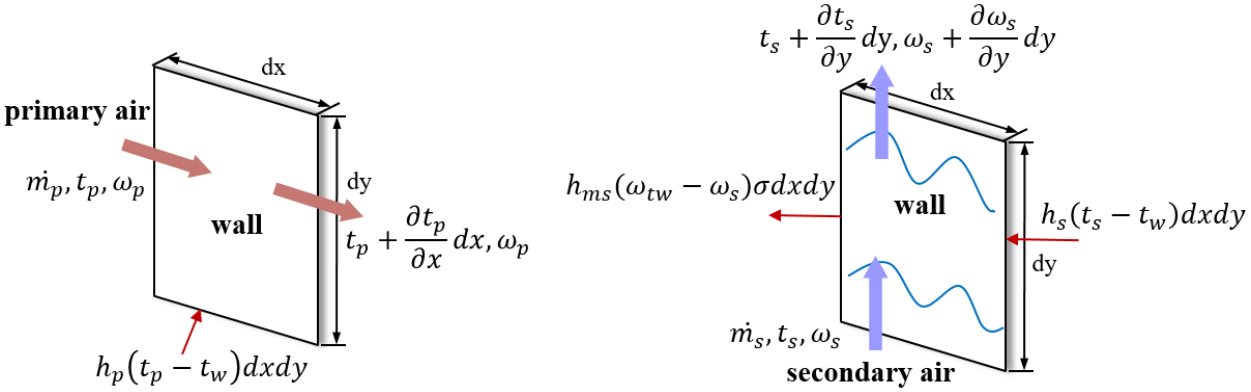

(a) differential element of the primary air side (b) differential element of the secondary air side

Fig. 3 Schematic view of elemental parts without condensation

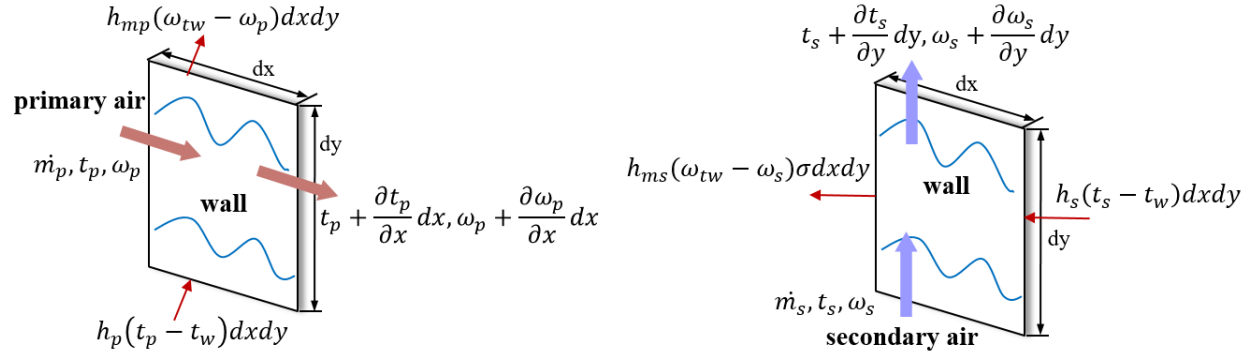

(a) differential element of the primary air side (b) differential element of the secondary air side

Fig. 4 Schematic view of elemental parts with condensation

The following Eqs. (1), (3-5), (7) constitute the enclosed governing equations of IEC when only sensible heat exchange takes place in the primary air channels. Conservation of energy and mass for the elements shown in Fig.3(a) and (b) are as follows.

For the energy balance of the secondary air:

$$h_s(t_w - t_s) \cdot dxdy + h_{fg}h_{ms}(\omega_{t_w} - \omega_s)\sigma \cdot dxdy = \dot{m}_s \frac{\partial i_s}{\partial y} \cdot dy \quad (1)$$

$$\dot{m}_s = (dx/L)m_s \quad (2)$$

For the mass balance of the secondary air:

$$h_{ms}(\omega_{t_w} - \omega_s)\sigma \cdot dxdy = \dot{m}_s \frac{\partial \omega_s}{\partial y} \cdot dy \quad (3)$$

For the mass balance of the evaporation water film:

$$\frac{\partial m_e}{\partial y} = \dot{m}_s \frac{\partial \omega_s}{\partial y} \quad (4)$$

For the heat balance of the primary air:

$$h_p(t_p - t_w) \cdot dxdy = c_{pa}\dot{m}_p \frac{\partial t_p}{\partial x} \cdot dx \quad (5)$$

$$\dot{m}_p = (dy/H)m_p \quad (6)$$

The energy balance of the control volume:

$$\dot{m}_s \frac{\partial i_s}{\partial y} - c_{pa}\dot{m}_p \frac{\partial t_p}{\partial x} = c_{pw}t_{ew} \frac{\partial m_e}{\partial y} \quad (7)$$

For the enthalpy of moist air ($i = c_{pa}t + h_{fg}^0\omega$) [34], c_{pa} is regard as a constant value of moist air in the flow direction to simplify the model [35]. The sensible heat gain of varied water vapor content is neglected under consideration of this study.

For total heat exchange conditions when the dew point temperature of the primary air is higher than local plate surface temperature, i.e., $t_{dew,p} > t_w$, the condensation will take place in the primary air channels with the moisture released from the primary air to plate surface. As the film thickness of condensation is thin and can be promptly drained away via gravity, the effect of heat conduction in the condensation film can be neglected [36, 37]. The conservation of the energy and mass for the elements with condensation are shown in Fig.4(a) and (b). In this case, the Eqs. (8-11) can replace Eqs. (5)(7) to represent the heat and mass balance equations of the control volume.

$$h_p(t_p - t_w) \cdot dxdy = c_{pa}\dot{m}_p \frac{\partial t_p}{\partial x} \cdot dx \quad (8)$$

$$h_{mp}(\omega_{t_w} - \omega_p) \cdot dxdy = \dot{m}_p \frac{\partial \omega_p}{\partial x} \cdot dx \quad (9)$$

$$\frac{\partial m_c}{\partial y} = -\dot{m}_p \frac{\partial \omega_p}{\partial x} \quad (10)$$

$$\dot{m}_s \frac{\partial i_s}{\partial y} - \dot{m}_p \frac{\partial i_p}{\partial x} = c_{pw}t_{ew} \frac{\partial m_e}{\partial y} + c_{pw}t_{cw} \frac{\partial m_c}{\partial y} \quad (11)$$

The average heat and mass transfer coefficients can be calculated according to a mathematical model developed by Ren and Yang [16]. In order to calculate the moisture content of saturated air at the plate

surface temperature, the following simplification is made according to the fitted relationship between plate surface temperature and saturated air humidity ratio [38]:

$$\ln(P_{q_b}) = \frac{a_1}{T_w} + a_2 + a_3 T_w + a_4 T_w^2 + a_5 T_w^3 + a_6 \ln(T_w) \tag{12}$$

$$\omega_{t_w} = 0.622 \frac{P_{q_b}}{B - P_{q_b}} \tag{13}$$

Where, $a_1 = -5800.2206$, $a_2 = 1.3914993$, $a_3 = -0.04860239$, $a_4 = -4.1764769 \times 10^{-5}$, $a_5 = -1.4452093 \times 10^{-8}$, $a_6 = 605459673$, $B = 101325Pa$ and 0℃ $< T_1 <$ 100℃.

The boundary conditions for the above governing equations are: **i**nlet primary air temperature, $t_p(\mathrm{x} = 0) = t_{p,in}$, **i**nlet primary air humidity ratio, $\omega_p(\mathrm{x} = 0) = \omega_{p,in}$, inlet condensation water mass rate, $m_c(\mathrm{x} = 0) = 0$, **i**nlet secondary air temperature, $t_s(\mathrm{y} = 0) = t_{s,in}$, **i**nlet secondary air humidity ratio, $\omega_s(\mathrm{y} = 0) = \omega_{s,in}$, inlet evaporative water mass rate, $m_e(\mathrm{y} = 1) = m_{e,in}$, where y=0 and y=1 are the points of bottom and top of the exchanger.

2.2 Numerical solution

The present sets of simultaneous partial differential and algebraic equations are nonlinear and cannot be solved analytically, so the finite difference method is used to discretize the governing equations. Central difference scheme is selected for its sufficient accuracy and stability, and the truncation error $\mathrm{O}(\Delta\chi^2)$ can be described as following:

$$\left(\frac{\partial T}{\partial x}\right)_{i,j} = \frac{T_{i+1,j} - T_{i-1,j}}{2\Delta x} + \mathrm{O}(\Delta\chi^2) \tag{14}$$

The simplified forms of the finite difference equations can be obtained as follows:

$$t_s(i+1,j) = t_s(i-1,j) + 2\Delta y NTU_s[t_w(i,j) - t_s(i,j)] \tag{15}$$

$$\omega_s(i+1,j) = \omega_s(i-1,j) + 2\Delta y \sigma NTU_{ms}[\omega_{t_w}(i,j) - \omega_s(i,j)] \tag{16}$$

$$t_p(i,j+1) = t_p(i,j-1) + 2\Delta x NTU_p[t_p(i,j) - t_w(i,j)] \tag{17}$$

$$\omega_p(i,j+1) = \omega_p(i,j-1) + 2\Delta x NTU_{mp}[\omega_p(i,j) - \omega_{t_w}(i,j)] \tag{18}$$

In the above equations,

$$NTU_s = \frac{h_s L}{c_{pa} m_s}, NTU_{ms} = \frac{h_{ms} L}{m_s}, NTU_p = \frac{h_p H}{c_{pa} m_p}, NTU_{mp} = \frac{h_{mp} H}{m_p}$$

By substitute the corresponding terms, the Eqs. (7)(11) can be transformed into algebraic equations without the partial differential items:

$$\frac{m_s}{m_p} \cdot NTU_s \cdot (t_w - t_s) + \frac{m_s h_{fg} - m_s c_{pw} t_{ew}}{m_p c_{pa}} \cdot NTU_{ms} \cdot \left(\omega_{t_w} - \omega_s\right) = NTU_p \cdot \left(t_p - t_w\right) \tag{20}$$

$$\frac{m_s}{m_p}\cdot NTU_s\cdot(t_w-t_s)+\frac{m_s h_{fg}-m_s c_{pw}t_{ew}}{m_p c_{pa}}\cdot NTU_{ms}\cdot\left(\omega_{t_w}-\omega_s\right)$$
$$=NTU_p\cdot\left(t_p-t_w\right)+\frac{h_{fg}-c_{pw}t_{cw}}{c_{pa}}\cdot NTU_{mp}\cdot(\omega_p-\omega_{t_w}) \quad (21)$$

As results, the partial differential equations (1), (3-5), (7) for the elements without condensation and PDEs (1), (3-4), (8-11) for the elements with condensation can be simplified as two sets of algebraic Eqs. (14-17), (20) and (14-19), (21). The simulation flow chart for solving the governing equations is shown in Fig. 5. With supplemented boundary conditions, the unique decision can be derived by an iterative method.

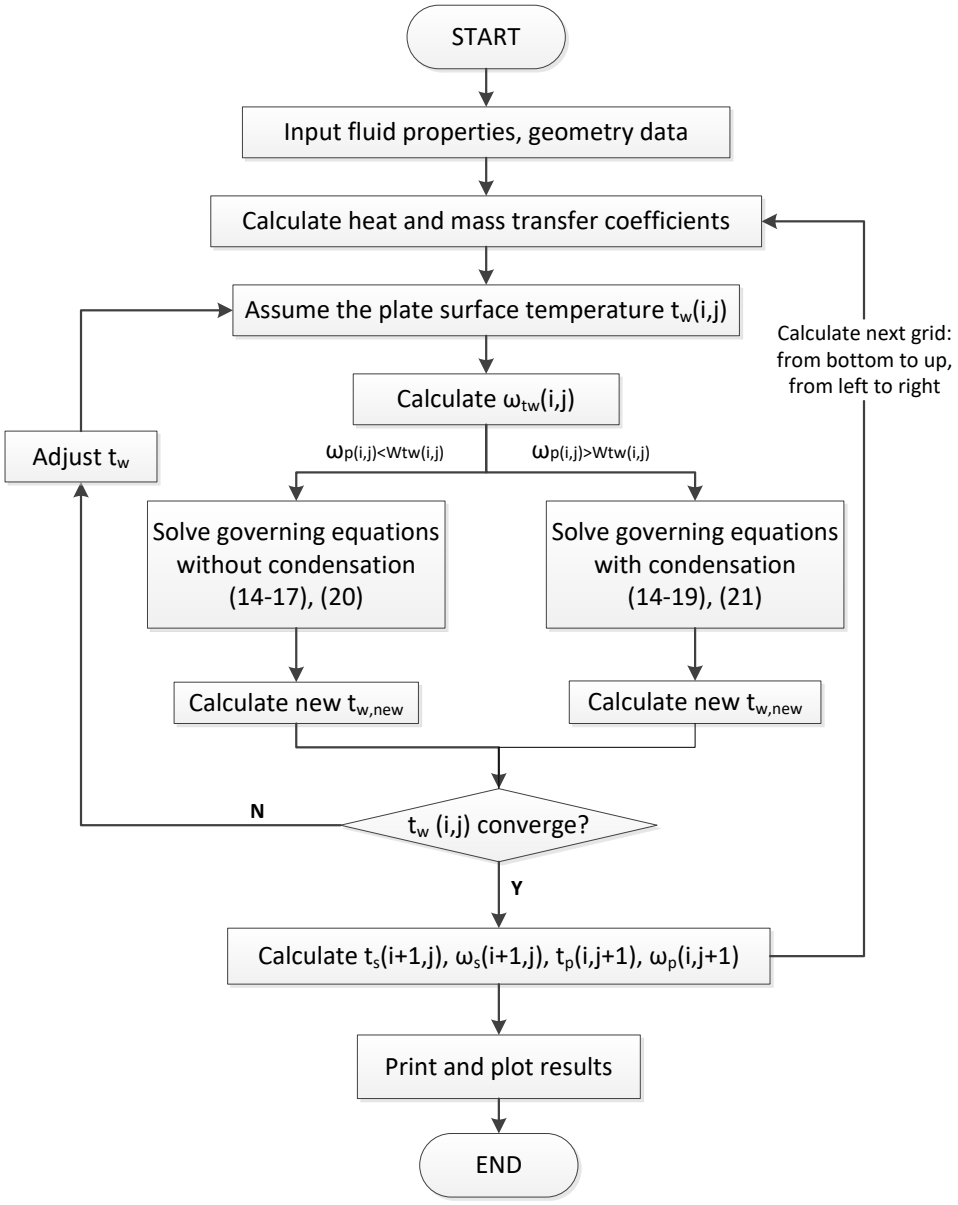

Fig. 5 Simulation flow chart for solving the IEC model.

In order to minimize the truncation error, the grid independence of developed models is checked by computing the identical variants on various space domain grid sizes. Simulations were conducted with grid size increasing from 20×20 to 200×200 so as to determine the optimum number of grid nodes when outlet primary air temperature and moisture content remains steady. As the results shown in Fig. 6, 100 elements were selected as the optimal grid number to achieve minimum computation time within the given tolerance of accuracy.

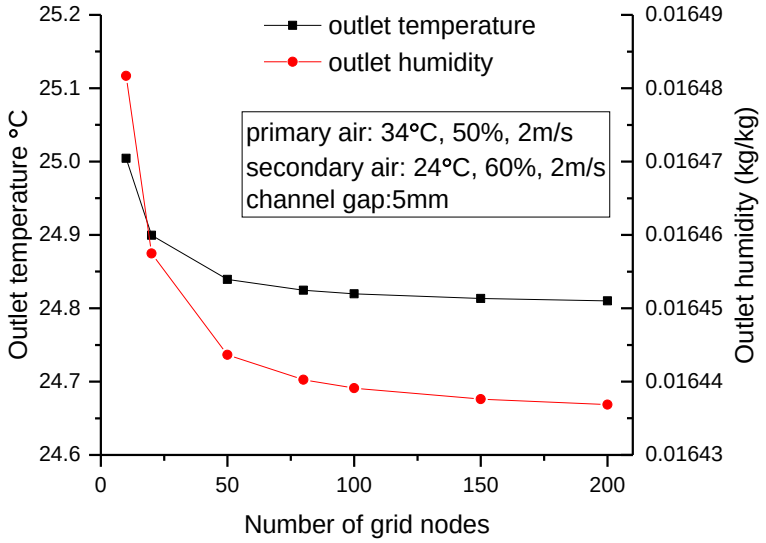

Fig. 6 Outlet parameters under different grid node numbers.

2.3 Evaluation indexes

2.3.1 Thermal performance

The evaluation indexes used for assessing the performance of IEC operated in hot and humid areas with possible condensation in the primary air channels should describe both the effects of sensible heat and total heat transfer. In this case, wet-bulb effectiveness η_{wb} is chosen for describing the ability of IEC in handing sensible heat, and total heat transfer rate per unit mass q_{tot} (kW/kg) is used to evaluate the total heat removed from the primary air or its enthalpy drop per unit mass [30]. The condensation ratio R_{con} represent the proportion of condensation area to the total heat exchanger area of coolers. They are expressed as:

$$\eta_{wb} = \frac{t_{p,in} - t_{p,out}}{t_{p,in} - t_{wb,s}} \tag{22}$$

$$q_{tot} = \frac{Q_{tot}}{M_p} = \frac{c_{pa} \cdot m_p \cdot \left(t_{p,in} - t_{p,out}\right) + h_{fg} \cdot m_p \cdot (\omega_{p,in} - \omega_{p,out})}{m_p \cdot (H/u_p)} \tag{23}$$

$$R_{con} = \frac{A_{con}}{A} \tag{24}$$

$$q_{sen} = \frac{Q_{sen}}{M_p} = \frac{c_{pa} \cdot m_p \cdot (t_{p,in} - t_{p,out})}{m_p \cdot (H/u_p)} \tag{25}$$

2.3.2 Energy consumption

Unlike conventional air-conditioning systems that consume electricity to drive the compressor, the IEC system only uses electrical power to run fan and pump. The energy consumption of the IEC can be estimated by the following equations. Some basic explanation of the terms and coefficient values with empirical formula were presented by Chen in Ref.[32].

The calculation of air pressure drop:

$$\Delta \mathrm{P} = \frac{f_{Re}}{Re} \cdot \frac{L}{d_e} \cdot \frac{\rho u^2}{2} \tag{26}$$

The power consumption of the fan:

$$P_{p,fan} = \frac{Q \times \Delta P}{3600 \times 1000 \times \eta_0 \times \eta_1} \times K \tag{27}$$

The power consumption of the water pump:

$$\mathrm{W} = m_w \cdot g \cdot H_{tot} \cdot K = m_w \cdot g \cdot (H_{nozzle} + H_{gravity} + H_{value}) \cdot K \tag{28}$$

In equation 28, m_w is the recirculation water flow rate; H_{tot} is the total head loss which includes the heat loss of gravity, nozzle and valves.

The energy consumption of cross flow IEC shall be calculated in the same way as that of counter flow IEC in terms of exhaust air fan and water pump, while they differed in the assigned value of hydraulic diameter (d_e) and channel length (L) on the supply air fan power calculation because of different air flow directions. With the changes of channel dimensions, there might be a trade-off between the efficiency improvement of heat transfer and the increasing pressure drop. To evaluate the IEC performance by an integrated consideration of heat transfer efficiency and energy consumption, a net energy saving (E_{net}, kW) is adopted as an evaluation index, which is given by:

$$E_{net} = E_{saving} - E_{fan} - E_{pump} \tag{29}$$

$$E_{saving} = \frac{Q_{saving}}{COP} = \frac{m_p \cdot (i_{p,in} - i_{p,out})}{COP} \tag{30}$$

In equation (29), E_{saving} is the energy saving achieved by IEC; E_{fan} is the energy consumption of supply air fan and exhaust air fan; E_{pump} is the energy consumption of circulation pump. In equation (30, Q_{saving} is the total heat recovery; COP is the overall coefficient of performance of a central cooling system [39], which is set to be 4.5 in this study.

3. Model validation

The accuracy of the newly developed cross-flow IEC model was validated using simulation data and experimental data from literature. Both operation states of IEC without condensation from the primary air and IEC with condensation from the primary air were investigated under the same inlet conditions in published data.

The proposed IEC model under conditions of only sensible heat transferred from the primary air was validated by Guo and Zhao's study [34] on cross flow IEC through a case study. By setting the specific inlet air conditions, unit geometry and heat transfer coefficient as given in the literature, the distributions of cross-sectional averaged temperature along the flow directions of primary air T_p, secondary air T_s, and the plate surface temperature T_w were compared. As shown in Fig. 7 (a), the two sets of data are well coincident for primary air temperature and plate surface temperature with the discrepancy of 0.9% and 1.7%. The discrepancy of secondary air temperature variations peaks at 3.6% when the temperature declines to low-point after entering in the channels.

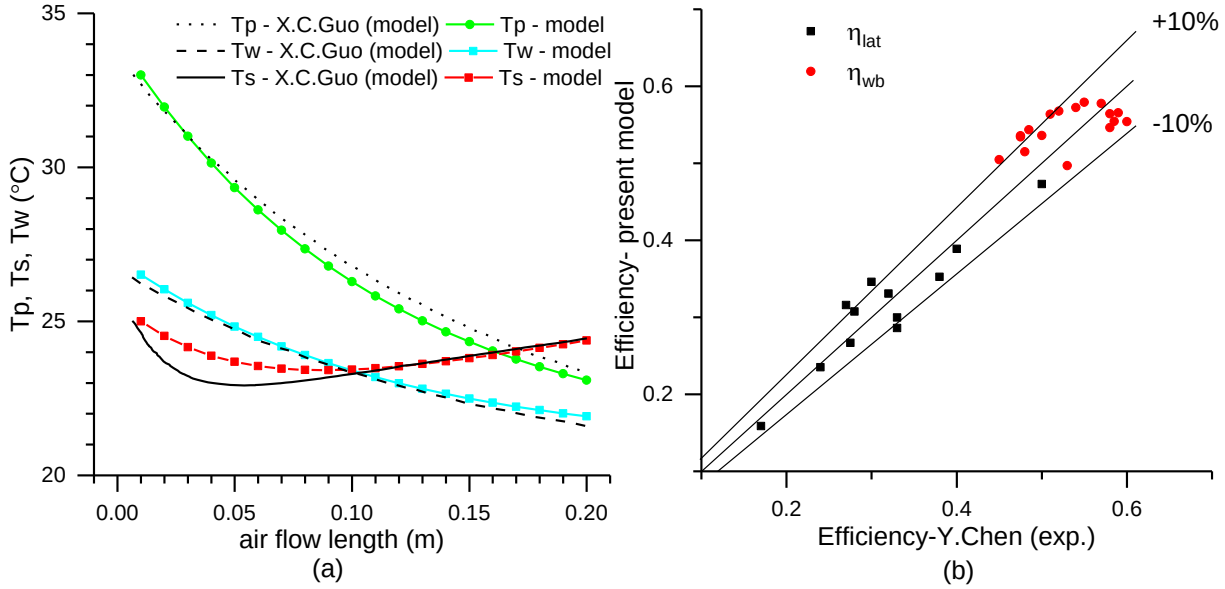

Fig. 7 Validation of the modeling results with published data. (a) temperature distributions at non-condensation state: $T_{pi} = 33℃, T_{si} = 25℃, RH_{si} = 70\%, \sigma = 1, s = 5mm, u_p = 3m/s$ and $u_s = 2.4m/s$. (b) efficiency at condensation states with various inlet conditions

Another verification of the present model under condensation state was conducted by comparing with the experimental results in Chen's study [40]. This paper investigated the performance of a plate type cross

flow air cooler which can be acted as an IEC under the wet operating mode. When the humidity of the inlet air is high, the condensation took place and the decreasing of primary air humidity were measured. The comparison between simulation data and experimental data are shown in Fig. 7(b). Both wet-bulb effectiveness η_{wb} and latent efficiency η_{lat} were simulated under the same input values of inlet air temperature and velocity as measured in the experiment. It was found that a discrepancy within 12% can be realized in predicting the efficiency of sensible heat and latent heat transfer, and the discrepancies for output values of primary air temperature and humidity were calculated within 2.8% and 1.8%.

4. Results and discussion

4.1 Temperature and humidity distribution

In order to present the air temperature and humidity distribution of cross flow IEC under condensation state, a case study was conducted at the inlet air properties and heat exchanger specifications of: $t_p = 34℃, RH_p = 50\%, u_p = 2m/s, t_s = 24℃, RH_s = 60\%, u_s = 2m/s, s = 5mm, H = 0.4m, L = 0.4m.$

As shown in Fig. 8, the secondary air enters in the channel at the temperature of 24℃, then it cools down with the evaporation process followed by a level off or a steep climb in temperature since the heat transferred from the primary air, especially on the boundary adjacent to the primary air inlet. The humidity ratio of secondary air keeps rising from 0.112 kg/kg (dry air) to an average value of 0.171 kg/kg (dry air) on the outlet boundary. The primary air flows to the channel horizontally at 34℃ and exits the exchanger with an average temperature decrease of 9.1℃. Combining Fig.8 (d) and (e), it's found that the condensation of primary air is closely related to plate temperature. It is observed that the humidity ratio begins to decrease when the plate temperature is below 22.1℃. The enthalpy drop of primary air is calculated to be 9.89 kJ/kg of which the latent heat accounts for 7.9%.

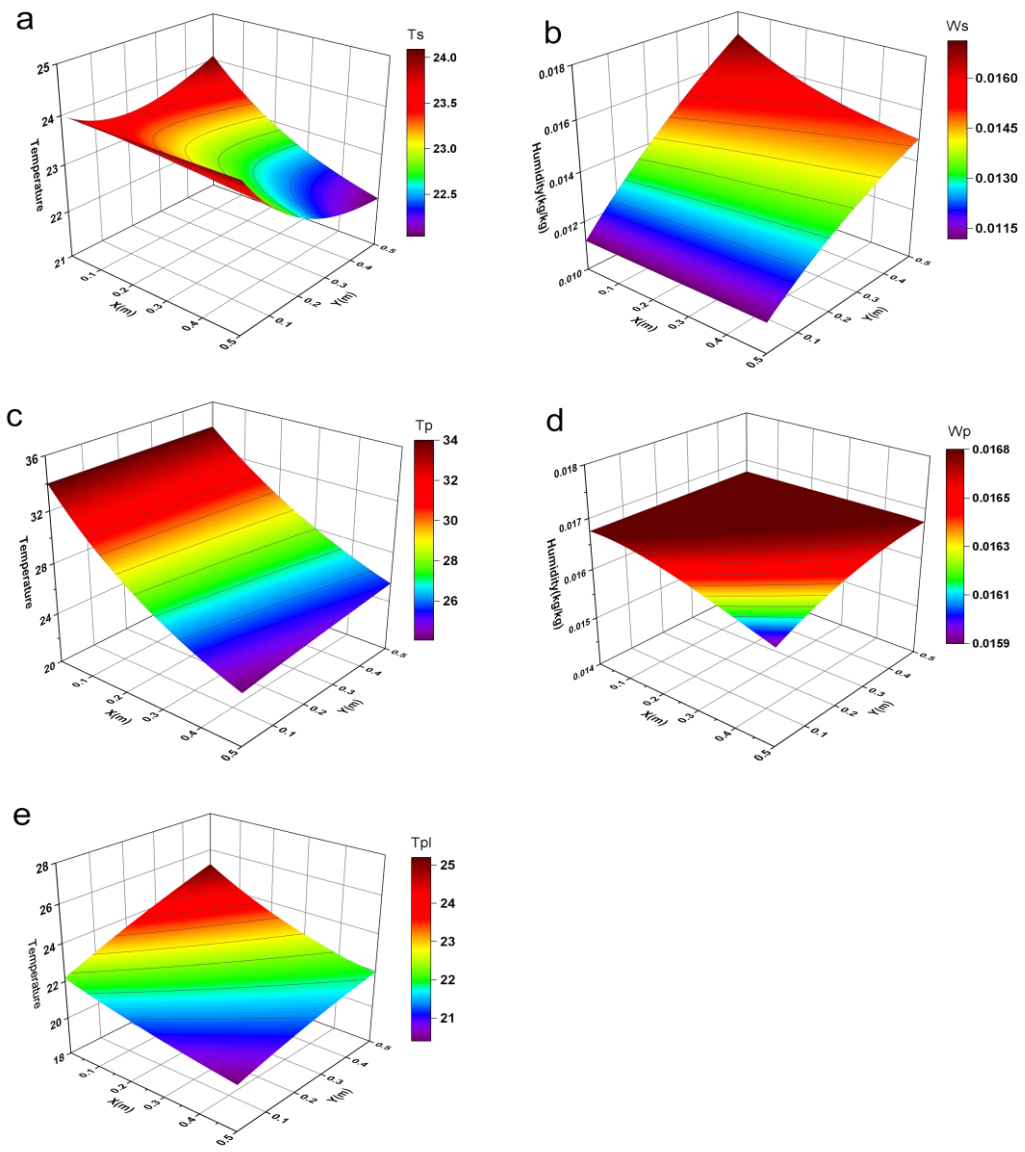

Fig. 8 Simulation results of temperature and humidity distribution across the exchanger (a: secondary air temperature, b: secondary air humidity, c: primary air temperature, d: primary air humidity, e: plate temperature)

4.2 Effect of inlet air properties

When the IEC is used as a precooling unit for fresh air in the hot and humid areas, the condensation in the primary air could probably take place as the higher humidity of the outdoor air. With the return air worked as secondary air with stable lower temperature, the IEC cooling performance is significantly affected by inlet primary air properties. In this section, three parameters including primary air temperature, humidity, and velocity were investigated by the developed cross flow and counter flow IEC models, in order to

analyze their influences on the performance of different IEC configurations under condensation conditions. The detailed arrangement of inlet primary air parameters for simulation conditions is listed out in Table 2. For each studied parameter, the value varied in a range (marked in bold) and the rest remained unchanged. The secondary air properties were set constantly as: t_s=26℃, RH_s=50%, u_s=2 m/s. Four evaluation indexes were calculated and compared between cross flow and counter flow IEC in the same physical size: wet-bulb efficiency η_{wb}, condensation ratio R_{con}, sensible heat transfer rate q_{sen} and total heat transfer rate q_{tot}.

Table 1. Pre-set operation conditions for simulation on air properties

Influence variables	Pre-set operation conditions		
	$t_{p,in}$ (℃)	$RH_{p,in}$	u_p (m/s)
$t_{p,in}$	**26-42**	0.6	3.0
$RH_{p,in}$	32	**0.3-0.9**	3.0
u_p	32	0.6	**0.5-5**

For each simulation condition: H=1m, L=1m, s=0.004m.

4.2.1 Temperature

Fig. 9 presents the influence of primary and secondary air temperature on the cooling performance of the IEC. The cross flow and counter flow IEC share the same variation trends in terms of R_{con}, $\eta_{wb,}$ and q_{tot}, while their differences change with the increasing inlet primary air temperature. The condensation ratio for both configurations keeps rising and it grows faster in counter flow configuration than in cross flow configuration. When $t_{p,in}$ increases to 36℃, the counter flow IEC is in total condensation state while the R_{con} in cross flow IEC is 0.82. Once condensation occurs, the web-bulb efficiency rises firstly and then decreases rapidly with the consequent heat release. Generally, the η_{wb} of counter flow configurations is higher than that of cross flow one, but the difference of η_{wb} between the two configurations narrow down from 6.8% to 2.4% with the difference on R_{con} growing up. Regarding the heat transfer rate, the sensible heat transfer rate of the two configurations keep an average difference of 1.6 kW/kg. However, the growth rate of q_{tot} is found to be more than two times larger than that of q_{sen} due to the latent heat release from condensation, and the difference between counter flow configuration is increasing continuously to 7.7 kW/kg at $t_{p,in}$=44.

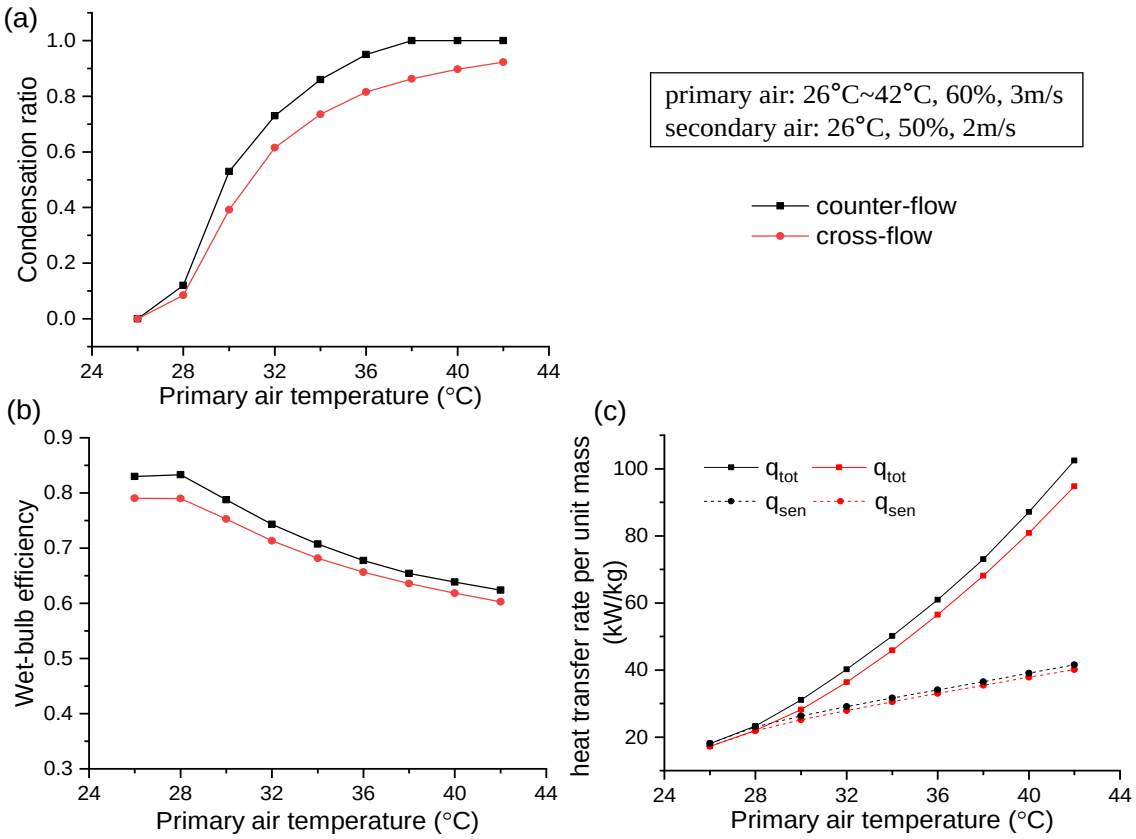

Fig. 9 Effect of inlet primary air temperature on cooling performance of cross flow and counter flow IEC. (a) Effect of $t_{p,in}$ on R_{con}. (b) Effect of $t_{p,in}$ on η_{wb}. (c) Effect of $t_{p,in}$ on q_{tot} and q_{sen}.

4.2.2 Humidity

Fig. 10 shows the effect of primary air humidity on cooling performance of counter flow and cross flow IEC. It is observed that the differences between the two configurations in η_{wb}, q_{sen} and q_{tot} are almost unchanged under non-condensation state and condensation state respectively with the increasing of $RH_{p,in}$. The condensation takes place at $RH_{p,in}$=0.45 for both configurations and then show a growing tendency. In a counter flow IEC, the total condensation is achieved when $RH_{p,in}$=0.7, while it does not appear in a cross flow IEC until $RH_{p,in}$=0.9. The simulated conditions of $RH_{p,in}$ from 0.45 to 0.9 in Fig. 9(b) are all under condensation states, in which the wet-bulb efficiency of both configurations drop steadily as condensation ratio increases. Under non-condensation states, the η_{wb} of counter flow heat exchanger is 6.3% higher than that of cross flow configuration on average. As the condensation takes place with the increase of $RH_{p,in}$, the difference of η_{wb} between two configurations narrows down to 2.3% when the largest gap of R_{con} between cross flow and counter flow exchangers occurs. As for q_{sen} and q_{tot}, the cross flow heat exchanger can offer cooling capacity 4.6% greater than cross flow one during non-condensation states when only sensible heat

transfer involved. After condensation occurs, the difference in q_{sen} between the two configurations decrease, while the difference in q_{tot} increase to 8.6% on average.

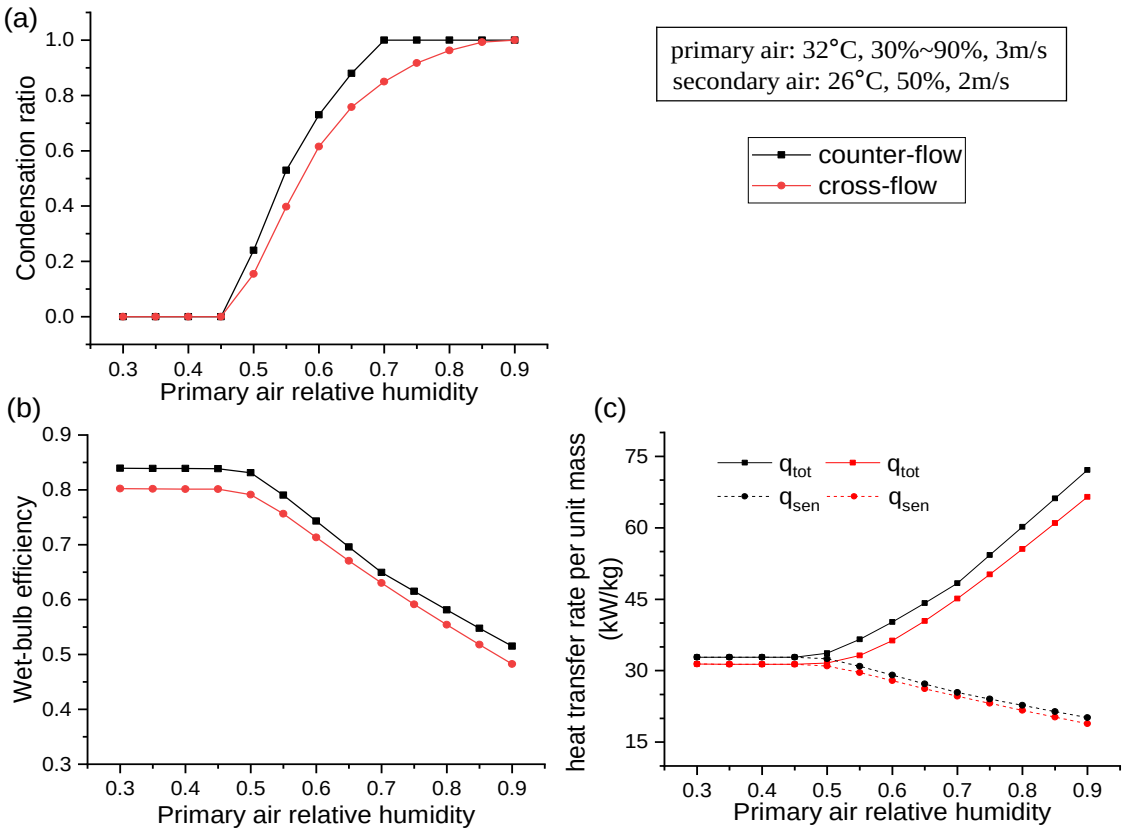

Fig. 10 Effect of inlet primary air humidity on cooling performance of cross flow and counter flow IEC. (a) Effect of $\omega_{p,in}$ on R_{con}. (b) Effect of $\omega_{p,in}$ on η_{wb}. (c) Effect of $\omega_{p,in}$ on q_{tot} and q_{sen}.

4.2.3 Velocity

Fig.11 presents the effect of primary air velocity on cooling performance of cross flow and counter flow IEC. It seems the increase of primary air velocity could extend the gaps between cross flow and counter flow IEC in R_{con}, $\eta_{wb,}$ and q_{tot} due to the rising primary air mass flow rate. As v_p increases from 0.5 m/s to 5 m/s, the difference in R_{con} between cross flow and counter flow exchangers grows up from 1.8% to 11.5%. Their difference in η_{wb} also increases from 1.6% to 6.4% at which the counter flow IEC could provide outlet primary air at average 0.6℃ lower than that of cross flow one. With regard to heat transfer, the q_{sen} presents linear growth with the increase of u_p, while a decreasing growth rate of q_{tot} is observed owing to the weakening of the condensation effect. The q_{tot} and q_{sen} in cross flow IEC rise more slowly than in counter flow arrangement, and the difference between the two configurations increase from 0.2 kW/kg to 5.7 kW/kg and from 0.1 kW/kg to 2.6 kW/kg, respectively.

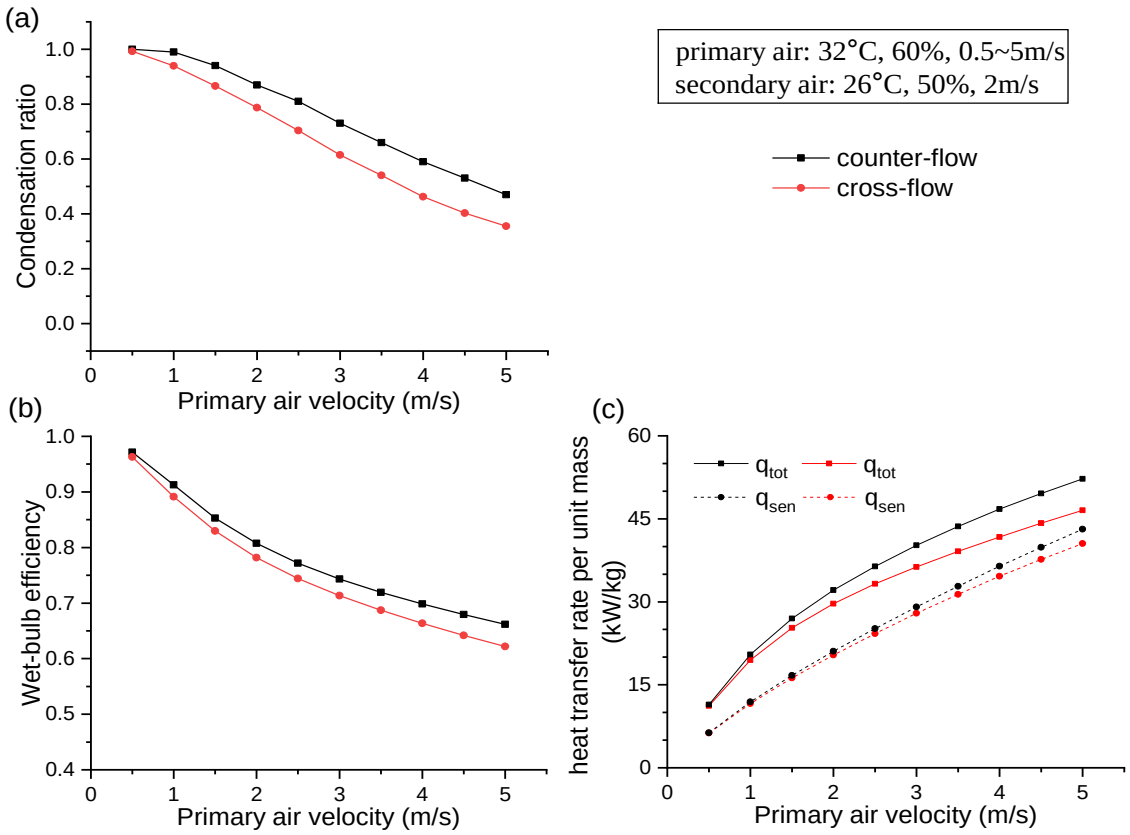

Fig. 11 Effect of inlet primary air velocity on cooling performance of cross flow and counter flow IEC. (a) Effect of $u_p$on R_{con}. (b) Effect of u_p on η_{wb}. (c) Effect of u_p on q_{tot} and q_{sen}.

4.3 Effect of geometric parameters

The geometric parameters of IEC have great influence on not only cooling performance but also energy consumption. It's essential to meet the cooling demand, and at the same time, minimize the energy consumption in IEC design. In this paper, three geometrical parameters were comparatively investigated between cross flow and counter flow in terms of energy performance. The three parameters include channel gap (s), number of transfer units (NTU_p) and height to length ratio (H/L). The parameter values for simulation setup are shown in Table 3. Three inlet primary air conditions are selected to represent the IEC operation conditions under non-condensation, partial condensation, and total condensation states. For each simulation condition, both the primary and secondary air flow volume are 800m^3/h, and the channels' number is 50. The variation of s, A, and H/L is in a range respectively as shown in Table 3. The heat exchange area (A) was represented by the dimensionless variable NTU_p, which ranges from 0.7 to 6 corresponding to the variation of plate area.

Table 2. Pre-set operation conditions for simulation on geometrical parameters

Influence variables	Pre-set operation conditions						
	t_p (℃)	RH_p	t_s (℃)	RH_s	s(mm)	A(m^2)	H/L
s (mm)	30	0.5	24	0.6	**2~9**	1	1
	35	0.5					
	35	0.8					
A(m^2)	30	0.5	24	0.6	4	**0.1-2**	1
	35	0.5					
	35	0.8					
H/L	30	0.5	24	0.6	4	1	**0.2~2.2**
	35	0.5					
	35	0.8					

4.3.1 Channel gap

According to Fig.12, as channel gap increases from 2 mm to 9mm, the cross flow and counter flow heat exchangers present the same trends of variation on η_{wb}, $q_{tot,}$ and E_{net} and the differences between them are decreasing. Under the inlet primary air condition of 35℃ and 50%, partial condensation state occurs both in cross flow and counter flow IEC. The condensation zones in cross flow pattern remain consistent while the R_{con} of counter flow IEC steadily decreases which results in their gaps are gradually narrowed down. For the inlet primary air condition of 35℃ and 80%, the η_{wb} is the lowest because of the heat released from total condensation state, and it decreases most rapidly (35%) in both two flow configurations with the expanding channel gap for the deteriorating heat and mass transfer performance.

It can be noticed in Fig. 12(c) that the highest total heat transfer rate is achieved when the channel gap is the smallest. When channel gap increases from 2 mm to 9 mm, especially for condensation conditions, the q_{tot} decreases dramatically and the difference between two flow configurations decreases from 4.3 kW/kg to 1.4 kW/kg as the downswing trend in q_{tot} of counter flow is more significant than that of cross flow. The q_{tot} represents the total heat transfer rate of which is improved with the decrease of channel gap for the more sufficient heat transfer between air flow and plate. However, the narrow channel gap can result in large pressure loss of air stream and more energy consumption of the fans. The energy consumption of the fan increases sharply when the channel gap is lower than 3mm. Net energy saving (E_{net}) is therefore proposed by considering both the total heat transfer rate and energy consumption of IEC presented in Fig. 12(d). The

optimal channel gap is reached when E_{net} reaches the peak point. It shows that the optimal channel gap ranges from 2 mm to 4 mm for both the cross flow and counter flow IEC under different inlet air conditions (2 mm (35℃, RH=80%), 3 mm (35℃, RH=50%), 4 mm (30℃, RH=50%)).

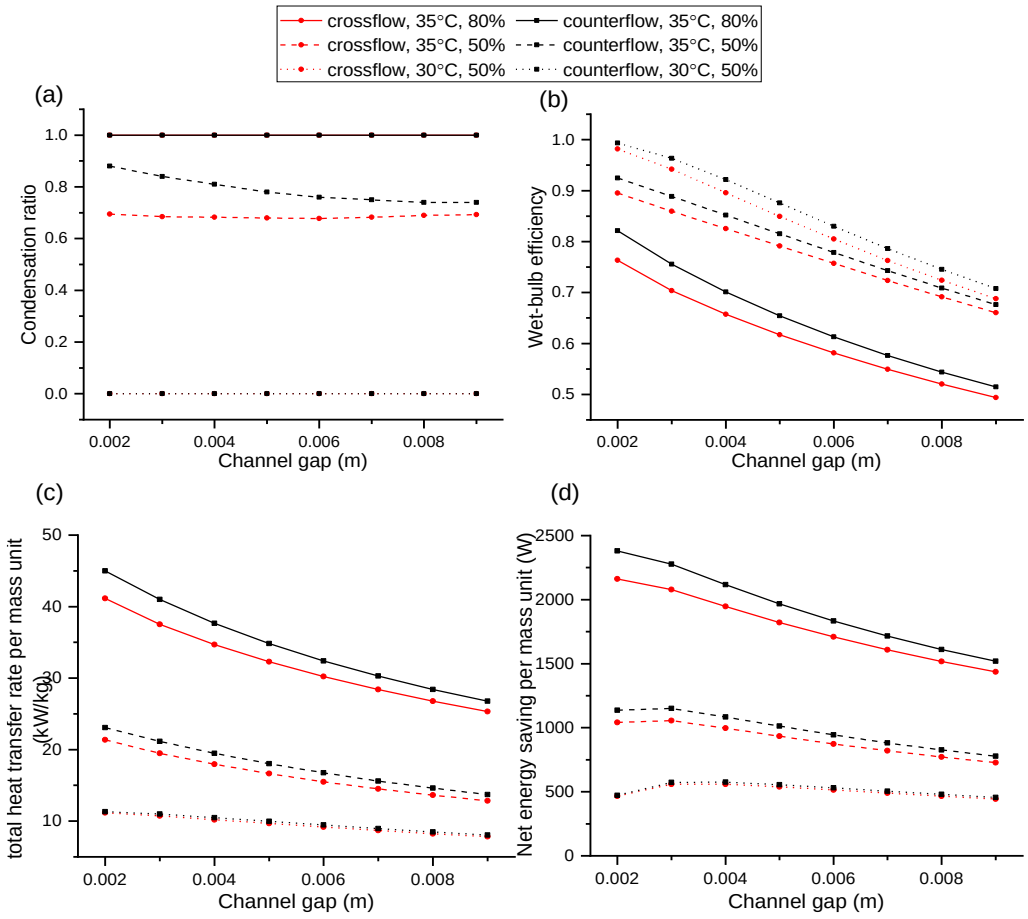

Fig. 12 Effect of channel gap on the energy performance of cross flow and counter flow IEC. (a) Effect of s on R_{con}. (b) Effect of s on η_{wb}. (c) Effect of s on q_{tot}. (d) Effect of s on E_{net}.

4.3.2 NTU_p

With the NTU_p increases from 0.7 to 6.0, the η_{wb}, q_{tot} and E_{net} are all improved because of the increasing heat and mass transfer area. As shown in Fig. 13(a), under partial condensation state, the R_{con} of both configurations decreases rapidly at first and then slows down until NTU_p increase to 2.4. Besides, the difference of R_{con} between cross flow and counter flow IEC increases with the rising NTU_p. Under the same inlet air conditions and NTU_p, the η_{wb} of counter flow IEC is higher than that of cross flow IEC. The average difference in η_{wb} between the two configurations is 2.3% under partial condensation state, which is lower than that of non-condensation state (4.2%) and total condensation state (5.5%). It is because that the higher

R_{con} of counter flow IEC in partial condensation state could lead to larger heat release and higher outlet air temperature which minimize the advantages over cross flow pattern.

In Fig. 13(c), there is a sharp increase in q_{tot} with the NTU_p rising from 0.7 to 3.1, after which the growth trend is slowed down gradually. The difference in q_{tot} between counter flow and cross flow IEC also goes up with the rising NTU_p, and their difference under total condensation state is the most significant, which increases from 0.3 to 2.3 kW/kg at NTU_p=6. The net energy saving is shown in Fig. 13(d) reflect the similar growing tendency with q_{tot}, According to the corresponding variation of heat exchange plate area, the E_{net} of cross flow can approach closely to that of counter flow one when NTU_p is lower than 3.1 ($A \leq 0.6m^2$). For operational conditions when $NTU_p \geq 3.1$, in order to achieve the same E_{net} with counter flow IEC, the plate area of cross flow should be 1.2~1.3 times larger than that of counter flow one.

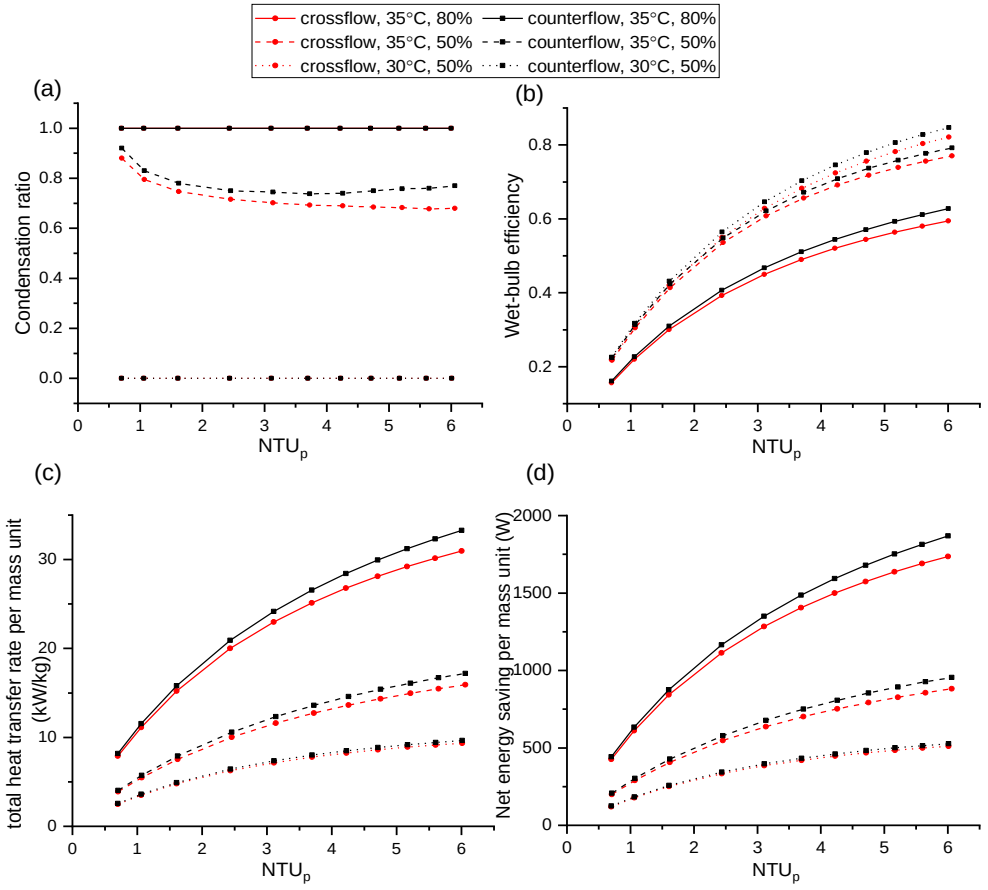

Fig. 13 Effect of NTU_p on the energy performance of cross flow and counter flow IEC.

(a) Effect of NTU_p on R_{con}. (b) Effect of NTU_p on η_{wb}.

(c) Effect of NTU_p on q_{tot}. (d) Effect of NTU_p on E_{net}.

4.3.3 Height to length ratio

The height to length ratio (H/L) of IEC heat exchanger is an important design index for coolers with definite plate area and air flow mass, but it has been rarely discussed in previous studies limited by only 1-D models of counter flow IEC were available. In this study, the H/L of cross flow and counter flow IEC were both investigated to compare their influence on cooling efficiency as well as energy consumption. It's observed in Fig. 14 that the two configurations show different variation trends on η_{wb}, q_{tot} and E_{net} with the increasing H/L. The η_{wb} of counter flow IEC increases with the rising H/L for the improved heat transfer length, and the upswing trend shows a level off after H/L increases to 0.8 due to larger air flow velocity and insufficient heat transfer process brought by smaller channel length. The η_{wb} of cross flow IEC shows contrary tendency that decreases with the increasing H/L which lead to weakened heat transfer length since the horizontal flow direction of primary air.

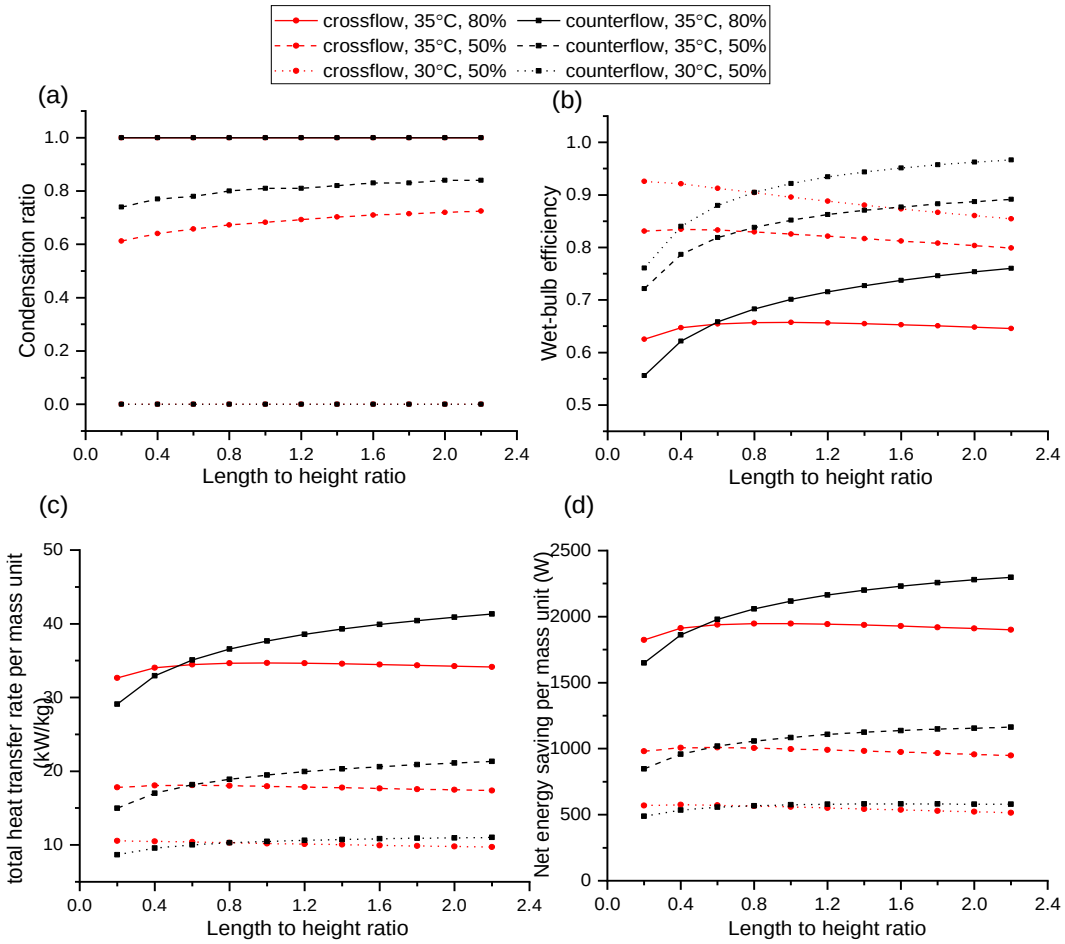

Fig. 14 Effect of height to length ratio on the energy performance of cross flow and counter flow IEC. (a) Effect of H/L on R_{con}. (b) Effect of H/L on η_{wb}. (c) Effect of H/L on q_{tot}. (d) Effect of H/L on E_{net}.

As Fig.14(c) (d) indicates, there is an intersection between cross flow and counter flow IEC in q_{tot} and E_{net} with the variation of H/L. The q_{tot} of counter flow IEC is lower than that of cross flow pattern at smaller H/L, and it keeps rising with the H/L increases from 0.2 to 2.2 and overtakes the q_{tot} of cross flow IEC eventually. The differences of the q_{tot} between two configurations converge to a point at H/L of 0.5 (35℃, 80%), 0.6 (35℃, 50%) and 0.8 (30℃, 50%) respectively under different inlet air conditions. The same comparative results are drawn for the E_{net} of two flow configurations, but the influence of energy consumption is significant at extreme H/L of which the channel is too narrow. The maximum E_{net} can be reached in cross flow IEC at H/L of 0.4 (30℃ and 50%), 0.6 (35℃ and 50%), 0.8 (35℃ and 80%) with different inlet air conditions.

5. Conclusions

By considering the possible condensation in the primary air when indirect evaporative cooler (IEC) is applied in hot and humid areas, this paper established a novel numerical 2-D model of cross flow IEC. Based on the validated model, the influences of operational parameters (inlet primary air temperature, humidity, velocity) on cooling performance were thoroughly compared between cross flow IEC and counter flow IEC under condensation state. Moreover, geometric parameters (channel gap, number of transfer units and height to length ratio) were varied under three operational conditions in order to find their differences on optimal design values under non-condensation state, partial condensation state and total condensation state. The main research results can be concluded as follows:

(1) The condensation ratio (R_{con}) of cross flow IEC is 2%~15% lower than that of counter flow IEC under the same operational conditions when partial condensation occurs. Due to the consequent heat release during condensation process, the higher R_{con} in counter flow IEC lead to a larger outlet air temperature rise than that of cross flow one, and the difference in η_{wb} between the two configurations narrows down from 7% (non-condensation state) to 2~3% (condensation state) on average.

(2) With the variation of operational conditions, the difference in sensible heat transfer rate (q_{sen}) between cross flow and counter flow IEC is maintained at 5% on average for both non-condensation and condensation states. Once the condensation occurs in primary air, the total heat transfer rate (q_{tot}) increases 2~3 times more rapidly than q_{sen}, and it is around 9% lower in cross flow than in counter flow.

(3) The optimal channel gap is 2 mm to 4 mm for both cross flow and counter flow IEC under condensation states. The advantages of counter flow IEC in q_{tot} over the cross flow IEC decreases from 4.3 kW/kg to 1.4 kW/kg when the channel gap increases from 2 mm to 9 mm.

(4) When the number of transfer units (NTU_p) of an IEC is lower than 3.1, the difference in net energy saving (E_{net}) between cross flow and counter flow could be less than 5%. When $NTU_p \geq 3.1$, their

difference increases steadily. The plate area of cross flow IEC should be 1.2~1.3 times larger than that of counter flow IEC to achieve the same energy saving.

(5) As the height to length ratio (H/L) increases, in contrast with the ever-growing q_{tot} of counter flow IEC, the q_{tot} of cross flow IEC show a short rise followed by a slight dip. The η_{wb}, q_{tot} and E_{net} of cross flow pattern are greater than those of counter flow pattern when the IEC is designed with small H/Ls: ≤0.5 for total condensation state, ≤0.6 for partial condensation state and ≤0.8 for non-condensation state.

Acknowledgement

The authors wish to acknowledge the financial supports provided by the Research Institute of Sustainable Urban Development of The Hong Kong Polytechnic University and the Housing Authority of the Hong Kong SAR Government.

References:

[1] H. Caliskan, I. Dincer, and A. Hepbasli, "Exergetic and sustainability performance comparison of novel and conventional air cooling systems for building applications," *Energy and Buildings,* vol. 43, no. 6, pp. 1461-1472, 2011/06/01/ 2011.

[2] D. Pandelidis and S. Anisimov, "Numerical analysis of the heat and mass transfer processes in selected M-Cycle heat exchangers for the dew point evaporative cooling," *Energy Conversion and Management,* vol. 90, pp. 62-83, 2015/01/15/ 2015.

[3] J. Lin, R. Z. Wang, M. Kumja, T. D. Bui, and K. J. Chua, "Multivariate scaling and dimensional analysis of the counter-flow dew point evaporative cooler," *Energy Conversion and Management,* vol. 150, pp. 172-187, 2017/10/15/ 2017.

[4] E. G. Cruz and E. Kruger, "Evaluating the potential of an indirect evaporative passive cooling system for Brazilian dwellings," *Building and Environment,* vol. 87, pp. 265-273, May 2015.

[5] Y. M. Xuan, F. Xiao, X. F. Niu, X. Huang, and S. W. Wang, "Research and application of evaporative cooling in China: A review (I) - Research," *Renewable & Sustainable Energy Reviews,* vol. 16, no. 5, pp. 3535-3546, Jun 2012.

[6] A. Hasan, "Going below the wet-bulb temperature by indirect evaporative cooling: Analysis using a modified ε-NTU method," *Applied Energy,* vol. 89, no. 1, pp. 237-245, 2012/01/01/ 2012.

[7] A. Ahmad, S. Rehman, and L. M. Al-Hadhrami, "Performance evaluation of an indirect evaporative cooler under controlled environmental conditions," *Energy and Buildings,* vol. 62, pp. 278-285, 2013/07/01/ 2013.

[8] S. Anisimov, D. Pandelidis, and A. Jedlikowski, "Performance study of the indirect evaporative air cooler and heat recovery exchanger in air conditioning system during the summer and winter operation," *Energy,* vol. 89, pp. 205-225, 2015/09/01/ 2015.

[9] T. Wen, L. Lu, C. Dong, and Y. Luo, "Development and experimental study of a novel plate dehumidifier made of anodized aluminum," *Energy,* vol. 144, pp. 169-177, 2018/02/01/ 2018.

[10] S. Anisimov and D. Pandelidis, "Numerical study of the Maisotsenko cycle heat and mass exchanger," *International Journal of Heat and Mass Transfer,* vol. 75, pp. 75-96, 2014/08/01/ 2014.

[11] Y. Chen, H. Yang, and Y. Luo, "Investigation on solar assisted liquid desiccant dehumidifier and evaporative cooling system for fresh air treatment," *Energy,* vol. 143, pp. 114-127, 2018/01/15/ 2018.

[12] X. Cui, B. Mohan, M. R. Islam, and K. J. Chua, "Investigating the energy performance of an air treatment incorporated cooling system for hot and humid climate," *Energy and Buildings,* vol. 151, pp. 217-227, 2017/09/15/ 2017.

[13] I. L. Maclainecross and P. J. Banks, "A GENERAL-THEORY OF WET SURFACE HEAT-EXCHANGERS AND ITS APPLICATION TO REGENERATIVE EVAPORATIVE COOLING," *Journal of Heat Transfer-Transactions of the Asme,* vol. 103, no. 3, pp. 579-585, 1981 1981.

[14] N. J. Stoitchkov and G. I. Dimitrov, "Effectiveness of crossflow plate heat exchanger for indirect evaporative cooling," *International Journal of Refrigeration-Revue Internationale Du Froid,* vol. 21, no. 6, pp. 463-471, Sep 1998.

[15] H. X. Yang, C. Q. Ren, and P. Cui, "Study on performance correlations of an indirect evaporative cooler with condensation from primary airflow," *Hvac&R Research,* vol. 12, no. 3, pp. 519-532, Jul 2006.

[16] R. Chengqin and Y. Hongxing, "An analytical model for the heat and mass transfer processes in indirect evaporative cooling with parallel/counter flow configurations," *International Journal of Heat and Mass Transfer,* vol. 49, no. 3, pp. 617-627, 2006/02/01/ 2006.

[17] S. De Antonellis, C. M. Joppolo, P. Liberati, S. Milani, and F. Romano, "Modeling and experimental study of an indirect evaporative cooler," *Energy and Buildings,* vol. 142, pp. 147-157, 2017/05/01/ 2017.

[18] T. Wen, L. Lu, H. Zhong, and C. Dong, "Experimental and numerical study on the regeneration performance of LiCl solution with surfactant and nanoparticles," *International Journal of Heat and Mass Transfer,* vol. 127, pp. 154-164, 2018/12/01/ 2018.

[19] G. Heidarinejad and S. Moshari, "Novel modeling of an indirect evaporative cooling system with cross-flow configuration," *Energy and Buildings,* vol. 92, pp. 351-362, Apr 1 2015.

[20] S. Moshari, G. Heidarinejad, and A. Fathipour, "Numerical investigation of wet-bulb effectiveness and water consumption in one-and two-stage indirect evaporative coolers," *Energy Conversion and Management,* vol. 108, pp. 309-321, 2016/01/15/ 2016.

[21] S. Moshari and G. Heidarinejad, "Analytical estimation of pressure drop in indirect evaporative coolers for power reduction," *Energy and Buildings,* vol. 150, pp. 149-162, 2017/09/01/ 2017.

[22] C. Zhan, Z. Duan, X. Zhao, S. Smith, H. Jin, and S. Riffat, "Comparative study of the performance of the M-cycle counter-flow and cross-flow heat exchangers for indirect evaporative cooling – Paving the path toward sustainable cooling of buildings," *Energy,* vol. 36, no. 12, pp. 6790-6805, 2011/12/01/ 2011.

[23] J. Woods and E. Kozubal, "A desiccant-enhanced evaporative air conditioner: Numerical model and experiments," *Energy Conversion and Management,* vol. 65, pp. 208-220, 2013/01/01/ 2013.

[24] B. Riangvilaikul and S. Kumar, "Numerical study of a novel dew point evaporative cooling system," *Energy and Buildings,* vol. 42, no. 11, pp. 2241-2250, 2010/11/01/ 2010.

[25] S. Anisimov, D. Pandelidis, A. Jedlikowski, and V. Polushkin, "Performance investigation of a M (Maisotsenko)-cycle cross-flow heat exchanger used for indirect evaporative cooling," *Energy,* vol. 76, pp. 593-606, Nov 1 2014.

[26] S. Anisimov, D. Pandelidis, and J. Danielewicz, "Numerical study and optimization of the combined indirect evaporative air cooler for air-conditioning systems," *Energy,* vol. 80, pp. 452-464, Feb 1 2015.

[27] S. Anisimov and D. Pandelidis, "Theoretical study of the basic cycles for indirect evaporative air cooling," *International Journal of Heat and Mass Transfer,* vol. 84, pp. 974-989, May 2015.

[28] Y. Wan, C. Ren, and L. Xing, "An approach to the analysis of heat and mass transfer characteristics in indirect evaporative cooling with counter flow configurations," *International Journal of Heat and Mass Transfer,* vol. 108, pp. 1750-1763, May 2017.

[29] Y. Wan, C. Ren, Z. Wang, Y. Yang, and L. Yu, "Numerical study and performance correlation development on counter-flow indirect evaporative air coolers," *International Journal of Heat and Mass Transfer,* vol. 115, pp. 826-830, Dec 2017.

[30] Y. Chen, H. Yang, and Y. Luo, "Indirect evaporative cooler considering condensation from primary air: Model development and parameter analysis," *Building and Environment,* vol. 95, pp. 330-345, Jan 2016.

[31] Y. Chen, Y. Luo, and H. Yang, "A simplified analytical model for indirect evaporative cooling considering condensation from fresh air: Development and application," *Energy and Buildings,* vol. 108, pp. 387-400, 2015/12/01/ 2015.

[32] Y. Chen, H. Yang, and Y. Luo, "Parameter sensitivity analysis and configuration optimization of indirect evaporative cooler (IEC) considering condensation," *Applied Energy,* vol. 194, pp. 440-453, 2017/05/15/ 2017.

[33] B. Halasz, "A general mathematical model of evaporative cooling devices," *Revue Générale de Thermique,* vol. 37, no. 4, pp. 245-255, 1998/04/01/ 1998.

[34] X. C. Guo and T. S. Zhao, "A parametric study of an indirect evaporative air cooler," *International Communications in Heat and Mass Transfer,* vol. 25, no. 2, pp. 217-226, Feb 1998.

[35] D. Pandelidis, S. Anisimov, and W. M. Worek, "Comparison study of the counter-flow regenerative evaporative heat exchangers with numerical methods," *Applied Thermal Engineering,* vol. 84, pp. 211-224, 2015/06/05/ 2015.

[36] J.-Y. San and C.-L. Jan, "Second-law analysis of a wet crossflow heat exchanger," *Energy,* vol. 25, no. 10, pp. 939-955, 2000/10/01/ 2000.

[37] S. Anisimov, A. Jedlikowski, and D. Pandelidis, "Frost formation in the cross-flow plate heat exchanger for energy recovery," *International Journal of Heat and Mass Transfer,* vol. 90, pp. 201-217, 2015/11/01/ 2015.

[38] ASHRAE., *ASHRAE handbook of fundamentals*. Mar Lin Book Company, 1985.

[39] X. Q. Kong, R. Z. Wang, and X. H. Huang, "Energy efficiency and economic feasibility of CCHP driven by stirling engine," *Energy Conversion and Management,* vol. 45, no. 9, pp. 1433-1442, 2004/06/01/ 2004.

[40] Y. Chen, H. Yang, and Y. Luo, "Experimental study of plate type air cooler performances under four operating modes," *Building and Environment,* vol. 104, pp. 296-310, 2016/08/01/ 2016.